Miridae control using sex-pheromone traps. Modeling, analysis and simulations

M. Djoukwe Tapi, Leïla Bagny-Beilhe, Yves Dumont

Version of Record: https://www.sciencedirect.com/science/article/pii/S146812181930954X
Manuscript_963adb5141882257bf4eb879205fd131

Miridae control using sex-pheromone traps. Modeling, analysis and simulations.

M. Djoukwe Tapi[a,b,h], L. Bagny-Beilhe[c,d], Y. Dumont[e,f,g,h]

[a] *Department of Mathematics and Computer Science, University of Douala, Cameroon*
[b] *UMI 209 IRD/UPMC UMMISCO, University of Yaounde I, Cameroon*
[c] *CIRAD, UPR Bioagresseurs, 30501 Turrialba, Costa Rica*
[d] *Bioagresseurs, Univ Montpellier, CIRAD, Montpellier, France*
[e] *CIRAD, UMR AMAP, F-34398 Montpellier, France*
[f] *Univ Montpellier, CIRAD, CNRS, INRAE, IRD, AMAP, Montpellier, France*
[g] *University of Pretoria, Department of Mathematics and Applied Mathematics Pretoria, South Africa*
[h] *EPITAG, LIRIMA, France*

Abstract

Cocoa mirid, *Sahlbergella singularis*, is known to be one of the major pests of cocoa in West Africa. In this paper, we consider a biological control method, based on mating disrupting, using artificial sex pheromones, and trapping, to limit the impact of mirids in plots. We develop and study a piece-wise smooth delayed dynamical system. Based on previous results, a theoretical analysis is provided in order to derive all possible dynamics of the system. We show that two main threshold parameters exist that will be useful to derive long term successful control strategies for different level of infestation. We illustrate and discuss our results when cacao pods production is either constant along the year or seasonal. To conclude, we provide future perspectives based on this work.

Key words: Pest control, Cocoa Pest, Control strategy, sex-pheromones, traps, Delay differential equations, Piecewise-smooth system, Monotone system, Stability analysis, Numerical simulation

1. Introduction

Mirids are responsible of several damages on cocoa in Africa, especially in Cameroon. Their presence leads to enormous losses of production and, thus, have an impact on trading and export. Losses due to mirids are difficult to estimate, but can reach $30-40\%$ of the potential production. Mirids are very harmful and can lead to the destruction of cocoa trees over the time. Development of pest management strategies are essential to prevent devastating impact on economy, food security, and biodiversity. Nowadays, in Cameroon, it is known that chemical control is the best ways to control mirid population. However, although chemical insecticides are very efficient to control mirids, their recurrent use is widely questioned due to their immediate adverse effects on the environment such as reduction of mirid natural enemies (impact on non targeted species), environmental pollution in ecosystems, resistance induction in the mirid population, and toxic effects on human health. In addition, these chemical products are very expensive. That is why the reduction of pesticides in cocoa production is becoming an important issue. In [1], we builded and studied several models (with and without delays) of mirids population and also several control strategies, including chemical treatment, mating disruption and trapping. We showed that the use of three applications of chemical treatment is equivalent to the combination of mating disruption and trapping. These two methods are less expensive and less toxic than chemical management and respect specific ecological and toxicological environmentally friendly requirements. In this paper, we will model more specifically the use of sex-pheromones to trap males and thus disturb matings, in order to eliminate or decay the population.

In Cameroon, different blends of the two components hexyl (R)-3-((E)-2-butenoyloxy)-butyrate and hexyl (R)-3-hydroxybutyrate) of the S. singularis female sex pheromone are used for tests. Traps used

*Corresponding author
Email address: yves.dumont@cirad.fr (Y. Dumont)

are delta or rectangular white-colored traps, made out of recycled polyethylene and cardboard. In a two years experiments [2], a total of 361 adults of *S. singularis* (359 males and two females) were caught. The highest numbers of mirids were found in traps with pheromone blends that combined a monoester and a diester. Rectangular traps also capture significantly more mirids than delta traps. Finally, in a recent work [3], the authors studied the impact of pheromone trap density (per ha) for cacao mirids mass trapping. It is clearly stated that this approach is a Male Annihilation Technique (MAT), with the objective of reducing the male population in order to lower the mirid population under an economical threshold.

In [1], the authors developed and studied several mirids population models, including a model with two delays. In [4], YD and co-authors developed and studied a piecewise smooth (PWS) system to model mating disrupting and trapping. Here, we propose to combine both approaches to develop and study a mathematical model to get a better understanding on the dynamics of the mirid population, under mating disruption and trapping. Then, the main objective of this work is to study the effort required in terms of sex-pheromone and trapping, to reduce the population size below harmful level. We obtain a piecewise smooth system of delayed differential equations. Using [1] and [4], we derive a system's analysis in order to provide a reliable and tractable strategy for a long time control. Since cocoa pods production in Cameroon is seasonal we also consider a periodic version of the delay PWS system. Finally, we provide numerical simulations to highlight the theoretical results and our reliable strategy.

The paper is organized as follows: in section 2, a sex-structured mirid model is built, based on [1] and [4]. In section 3, like in [4], mating disruption and trapping are included in the sex-structured model ; an analysis is provided that allows to build a useful control strategy, that is also illustrated by numerical simulations. Finally, in section 4, we consider the periodic case. The paper ends with a conclusion where we discuss possible extensions of this work.

2. A sex-structured model of mirid population

We consider a generic delayed model to describe the dynamics of *S. singularis*. The flow diagram is represented in Fig. 2, page 3. Based on biological and behavioral assumptions, we consider two main developments stages: eggs (E) and adults (females F and A, and male M). Indeed, after being laid, the eggs need, on average, $\tau_1 = 15$ days to become nymphs. These nymphs need $\tau_2 = 25$ days to complete the nymph's development and become adult males or females. After emergence, sexually mature female mate with males (attracted by sex pheromones released by the females) and then they need approximately $\tau_3 = 10$ days before being able to deposit eggs (in fact this is the time needed for the appearance of mature eggs in the ovarioles [5]). This is summarized in Fig.1, page 3.

We denote by $e^{-\tau_2 \mu_L}$ the proportion of nymphs respectively which survive the nymph stage. After mating, F becomes mated females, A, that need an additional period of maturation, τ_3, in order to lay eggs [5]. However, only a proportion, $e^{-\tau_3 \mu_A}$, of A females will deposit eggs. Thus, we have four compartments for our delayed model: E, the eggs' compartment, F, the sex-immature females compartment, A, the mated females compartment, and M, the males compartment.

Females release pheromone in order to attract males for mating. The mating between males and females is modeled as in [4]: as long as the male density is such that $\gamma M \geq F$, then all Females F will be inseminated and move to the compartment A, at rate ν_F. In contrary, if, for any reason, the male density is scarce, i.e. $\gamma M < F$ then the number of females F that will move to the compartment A is related to the number of Males, M. The other parts of the compartmental model follow the model developed in [1].

The biological parameters are described as follows: r is the sex ratio; b is the mean number of eggs laid by an adult female mirid per day that have emerged as nymphs, K_C is the maximal carrying capacity related to the mean daily number of pods per area (ha), μ_E, μ_M, μ_F and μ_A represents respectively the eggs, male, females daily mortality rate, ν_E is the transition rate from the egg to the next stage; $1/(\nu_E + \mu_E)$ is the mean time a mirid stays in the egg stage (measured in days); ν_F is the transition rate from the sex-immature female stage to mature female stage;

As already explained in [1], the non linear term $r\, b\, A \left(1 - \frac{E}{K_C}\right)$ is related to a skip-oviposition behavior. Indeed, according to expert's knowledge, mirids (*S. singularis*) are able to select their breeding sites according to their level of occupation.

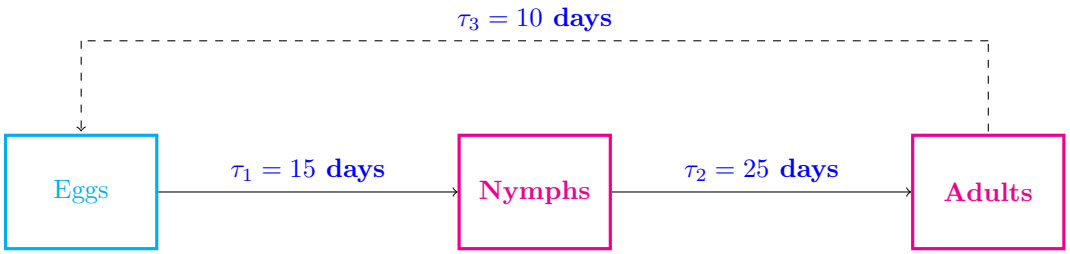

Figure 1: Life cycle of *S. singularis*

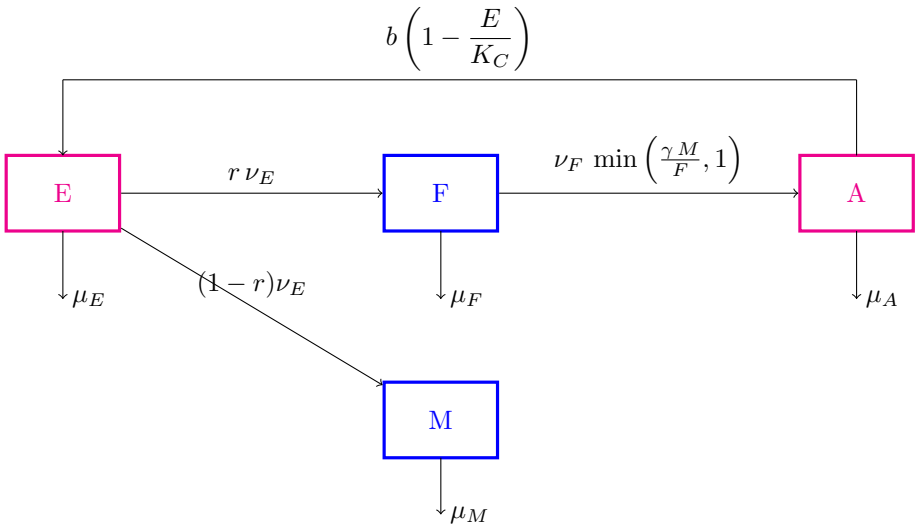

Figure 2: *Sahlbergella singularis* flow diagram with mating.

According to the diagram given in Fig. 2, we derive the following Delay Differential system

$$\begin{cases} \dot{E}(t) = b\,e^{-\tau_3\,\mu_A}\,A(t-\tau_3)\left(1-\dfrac{E(t)}{K}\right) - (\nu_E+\mu_E)\,E(t), \\ \dot{F}(t) = r\,\nu_E\,e^{-\tau_2\,\mu_L}\,E(t-\tau_2) - \nu_F\ \min\left(\dfrac{\gamma\,M(t)}{F(t)},1\right)\,F(t) - \mu_F\,F(t), \\ \dot{A}(t) = \nu_F\ \min\left(\dfrac{\gamma\,M(t)}{F(t)},1\right)\,F(t) - \mu_A\,A(t), \\ \dot{M}(t) = (1-r)\,\nu_E\,e^{-\tau_2\,\mu_L}\,E(t-\tau_2) - \mu_M\,M(t). \end{cases} \tag{1}$$

The parameters of model (1) are summarized in Table 1, page 4.

3. Control using mating disruption and trapping

In order to maintain a low level a mirid population, we consider a control using sex pheromone traps. The objective is to disrupt the mating by the use of female pheromones, but also to reduce the number of males, by trapping, in order to reduce the overall population. However, to model the pheromones, like in [4], we assume that the release of pheromones is equivalent to the releases of "Fake Females", F_p, such that our approach can be somehow linked to the Sterile Insect Technique (SIT) approach, where sterile males are released to disrupt the mating between wild males and females in order to reduce the number of offsprings and so on (see for instance [6–8] for an overview and results on SIT).

Because of the release of Fake female, F_p, the mating term in the previous system becomes $\min\left(\dfrac{\gamma\,M(t)}{F(t)+F_p},1\right)$, such that if the number of Fake females is large enough then $\dfrac{\gamma\,M(t)}{F(t)+F_p} < 1$. Clearly when the mirid

Table 1: Parameters of model (1).

Parameters	Biological significance	Unit
b	Mean daily number of eggs laid by a mature female	days^{-1}
r	sex ratio	-
K	Maximal carrying capacity related to the mean daily number of pods per ha	eggs^{-1}
ν_F	daily rate from F to A	days^{-1}
μ_A	death rate of adults females	days^{-1}
μ_M	death of adults males	days^{-1}
μ_F	death of sexual immature females	days^{-1}
μ_E	death rate of eggs	days^{-1}
$1/\nu_E$	Time necessary for an egg to change its stage	days
α	The maximal death rate by sex-pheromone trap	days^{-1}
γ	daily number of females that can be inseminated by a single male	-
$\tau_1 = \dfrac{1}{\nu_E}$	average time needed for eggs to become nymphs	days
τ_2	average time needed for nymphs to become adults	days
τ_3	average maturation time needed by mated females to deposit eggs	days

population is large, a large number of Fake females is necessary to impact the mating. When Fake females are not released in sufficient numbers, then, the control will have no effect on an established (and large) mirid population. The parameter α represents the maximum capture rate by trapping, the ratio $\dfrac{F_p}{F+F_p}$ represents the attractiveness of the traps. The new flow diagram is represented in Fig. 3, page 4. According to the flow diagram given in Fig. 3, page 4, and taking into account the life cycle of *S.*

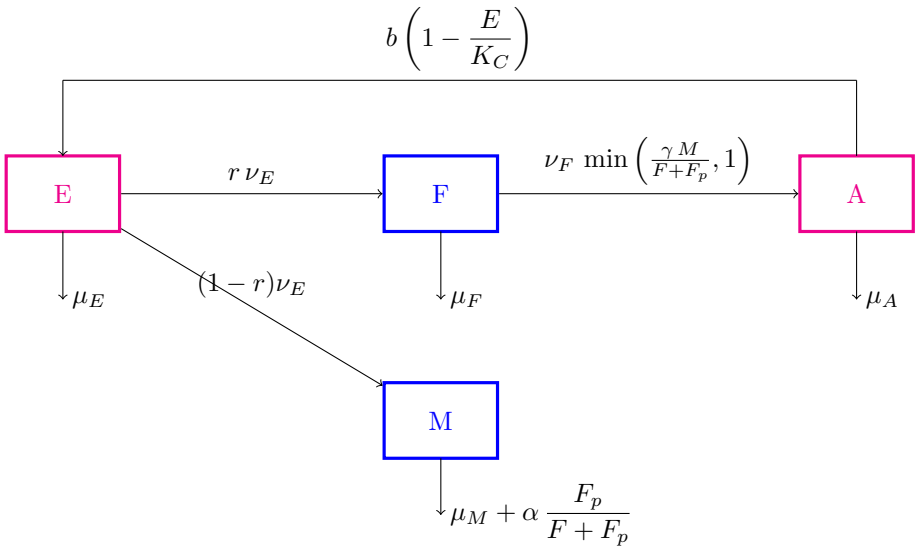

Figure 3: *Sahlbergella singularis* control model using sex pheromone traps.

singularis, we obtain a new mating disruption and trapping control model

$$\begin{cases} \dot{E}(t) = b\, e^{-\tau_3\,\mu_A}\, A(t-\tau_3)\left(1-\dfrac{E(t)}{K}\right) - (\nu_E+\mu_E)\, E(t), \\ \dot{F}(t) = r\,\nu_E\, e^{-\tau_2\,\mu_L}\, E(t-\tau_2) - \nu_F\, \min\left(\dfrac{\gamma\, M(t)}{F(t)+F_p}, 1\right) F(t) - \mu_F\, F(t), \\ \dot{A}(t) = \nu_F\, \min\left(\dfrac{\gamma\, M(t)}{F(t)+F_p}, 1\right) F(t) - \mu_A\, A(t), \\ \dot{M}(t) = (1-r)\,\nu_E\, e^{-\tau_2\,\mu_L}\, E(t-\tau_2) - \left(\mu_M + \alpha\dfrac{F_p}{F(t)+F_p}\right) M(t). \end{cases} \tag{2}$$

Model (2), like model (1), enters the family of piece-wise dynamical systems with delay differential equations (shortly, PWS-DDE) (See Appendix A).
The switching manifold is defined as follows

$$\sum := \left\{ x \in \mathbb{R}^4_+, \quad F + F_p = \gamma\, M \right\}$$

Model (2) can be rewritten in the form:

$$\frac{dx}{dt} = f(x, x_\tau) := \begin{cases} f_1(x, x_{\tau_2}, x_{\tau_3}) & if \quad F + F_p \le \gamma\, M \\ f_2(x, x_{\tau_2}, x_{\tau_3}) & if \quad F + F_p \ge \gamma\, M \end{cases} \tag{3}$$

where $x = (E, F, A, M)^t$, $x_{\tau_2} = x(t-\tau_2)$, $x_{\tau_3} = x(t-\tau_3)$,

$$f_1(x, x_\tau) = \begin{pmatrix} b\, e^{-\tau_3\,\mu_A}\, A(t-\tau_3)\left(1-\dfrac{E(t)}{K}\right) - (\nu_E+\mu_E)\, E(t) \\ r\,\nu_E\, e^{-\tau_2\,\mu_L}, E(t-\tau_2) - (\nu_F+\mu_F)\, F(t) \\ \nu_F\, F(t) - \mu_A\, A(t) \\ (1-r)\,\nu_E\, e^{-\tau_2\,\mu_L}\, E(t-\tau_2) - \left(\mu_M + \alpha\dfrac{F_p}{F(t)+F_p}\right) M(t) \end{pmatrix} \tag{4}$$

and

$$f_2(x, x_\tau) = \begin{pmatrix} b\, e^{-\tau_3\,\mu_A}\, A(t-\tau_3)\left(1-\dfrac{E(t)}{K}\right) - (\nu_E+\mu_E)\, E(t) \\ r\,\nu_E\, e^{-\tau_2\,\mu_L}\, E(t-\tau_2) - \nu_F\gamma\dfrac{M(t)}{F(t)+F_p}\, F(t) - \mu_F\, F(t) \\ \nu_F\,\gamma\dfrac{F(t)}{F(t)+F_p}\, M(t) - \mu_A\, A(t) \\ 1-r)\,\nu_E\, e^{-\tau_2\,\mu_L}\, E(t-\tau_2) - \left(\mu_M + \alpha\dfrac{F_p}{F(t)+F_p}\right) M(t) \end{pmatrix} \tag{5}$$

When $\tau_2 = \tau_3 = 0$, system (3) is exactly the same system studied in [4]. We will now consider the methodologies developed in [4] and [1] to study system (3).
Like in [4], the theoretical analysis of the model is carried out for two cases: male abundance and male scarcity. These two cases are separated by the hyperplane Σ. The analysis of the two systems can be carried out independently on the orthant $\mathbb{R}^4_+$. The obtained results will be merged into a general theorem for system (3) (or (2)).

3.1. Case with Male abundance: $\gamma\, M > F + F_p$

In this case, system (3) becomes

$$\frac{dx}{dt} = f_1(x, x_\tau). \tag{6}$$

Note that the right hand side of system (6), f_1, is continuous and Lipschitzian in x. Thus, according to the standard theory of delay differential equations [9], for each continuous initial condition $\psi \in \mathcal{C}\left([-\tau, 0], \mathbb{R}^4\right)$, where $\tau = \max\{\tau_2, \tau_3\}$, uniqueness and local existence of the solution are guaranteed. Note also, that, without delay, we recover the cooperative system studied in [4].

As explained in [1], some cooperative systems with delay can enjoy some nice properties such that their long term behavior is similar to the cooperative system without delay. Let $Y = (x(t-\tau_3), x(t-\tau_2))$, $x = (E, F, A, M)^T$. System (6) verifies the, so-called, quasimonotone (QM) condition [10], if

(a) $\dfrac{\partial f_{1,i}}{\partial x_j} \geq 0$ for $i \neq j$

(b) $\dfrac{\partial f_{1,i}}{\partial Y_j^k} \geq 0$ for all i, j, k.

Condition (a) is verified since the non delayed model is a cooperative system. Let us verify condition (b):

$$\frac{\partial f_{1,1}}{\partial Y_3^1} = b\, e^{-\tau_3\, \mu_A} \left(1 - \frac{E(t)}{K}\right) \geq 0, \quad \frac{\partial f_{1,j}}{\partial Y_j^1} = 0 \quad \forall\ j = 1, 2, 4.$$

$$\frac{\partial f_{1,2}}{\partial Y_2^1} = r\, \nu_E\, e^{-\tau_2\, \nu_L}\, e^{-\tau_3\, \mu_F} \geq 0, \quad \frac{\partial f_{2,j}}{\partial Y_j^1} = 0 \quad \forall\ j = 2, 3, 4,$$

$$\frac{\partial f_{3,j}}{\partial Y_j^1} = 0 \quad \forall\ j = 1, 2, 3, 4,$$

$$\frac{\partial f_{1,4}}{\partial Y_1^1} = (1-r)\, \nu_E\, e^{-\tau_2\, \nu_L} \geq 0, \quad \frac{\partial f_{4,j}}{\partial Y_j^1} = 0 \quad \forall\ j = 2, 3, 4.$$

Then the (QM) condition is verified. This implies that if the initial condition is non negative (with at most one zero component) then the solution of system (6) is still non negative i.e $x(t) \geq 0$. Moreover, the (QM) condition guarantees the stability of each equilibrium of the non delayed system is preserved for the delayed system. In other words, it suffices to study the following non delayed system

$$\frac{dx}{dt} = f_1(x), \tag{7}$$

to deduce the behavior of the time delayed system (6). As already emphasized, system (7) has already been studied in [4], using [10, 11].
Setting

$$\mathcal{R} = \frac{r\, b\, \nu_E\, \nu_F\, e^{-\tau_2\, \mu_L}\, e^{-\tau_3\, \mu_A}}{\mu_A\, (\nu_E + \mu_E)\, (\nu_F + \mu_F)} \tag{8}$$

the so-called basic offspring number, and applying Theorem 9 [4] we deduce

Theorem 3.1. *(i) System (7) defines a positive dynamical system on $\mathbb{R}^4_+$.*

(ii) System (7) always has a trivial equilibrium, $\mathbf{0} = (0, 0, 0, 0)$, which is globally asymptotically stable when $\mathcal{R} \leq 1$.

(iii) When $\mathcal{R} > 1$, system has an additional positive equilibrium $X^* = (E^*, F^*, A^*, M^*)$ where

$$E^* = \left(1 - \frac{1}{\mathcal{R}}\right) K, \quad F^* = \frac{r\, \nu_E\, e^{-\tau_2 \mu_L}}{(\nu_F + \mu_F)} \left(1 - \frac{1}{\mathcal{R}}\right) K,$$

$$A^* = \frac{r\, \nu_E e^{-\tau_2 \mu_L}\, \nu_F}{\mu_A\, (\nu_F + \mu_F)} \left(1 - \frac{1}{\mathcal{R}}\right) K, \quad M^* = \frac{M^0}{\mu_M + \dfrac{\alpha\, F_p}{F^* + F_p}}$$

with

$$M^0 = (1-r)\, \nu_E e^{-\tau_2 \mu_L} \left(1 - \frac{1}{\mathcal{R}}\right) K.$$

Moreover, X^*, is also globally asymptotically stable when $\mathcal{R} > 1$ on

$$\mathbb{R}^4_+ \setminus \{\mathbf{0}\} = \mathbb{R}^4_+ \setminus \{\mathbf{x} \in \mathbb{R}^4_+ : \mathbf{E} = \mathbf{F} = \mathbf{A} = \mathbf{M} = \mathbf{0}\}.$$

Remark 3.1. *When $\alpha = 0$, we recover the positive equilibrium when no control occurs. It is important to notice that the effect on the control only impact the value of the Male equilibrium.*

The positive equilibrium X^* is called a regular (virtual) equilibrium of model (7) if and only if $F^* + F_p < (>)\gamma M^*$ which is equivalent to $F_p < F_p^*$, where

$$F_p^* = \frac{1}{\mu_M + \alpha}\left(\gamma M^0 - \mu_M F^*\right) = \frac{\nu_E e^{-\mu_L \tau_2}}{(\alpha + \mu_M)}\left[\gamma(1-r) - \frac{r\,\mu_M}{(\nu_F + \mu_F)}\right] E^*. \tag{9}$$

Therefore, we deduce that

- If $F_p < F_p^*$, the positive equilibrium X^* is a regular equilibrium of (7).
- If $F_p > F_p^*$, the positive equilibrium X^* is a virtual equilibrium of (7).

The threshold F_p^* determines the minimum level of control, i.e. the number of Fake females and thus, indirectly, the number of pheromones traps, below which the control has essentially no effect on an established mirid population. More precisely, as stated in the previous remark, the effect of pheromone traps is only limited to the males compartment (male trapping), all other compartments remain at their natural equilibrium. Thus females will continue to deposit as many eggs (inside pods) as before the control.

Thus, thanks to the (QM) condition, and, using Theorem 3.1, we deduce the following results in the DDE "male abundance" case:

Theorem 3.2. *(i) System (6) defines a positive dynamical system on $\mathbb{R}^4_+$.*

(ii) System (6) always has one equilibrium, $\mathbf{0}$, that is globally asymptotically stable when $\mathcal{R} \leq 1$.

(iii) When $\mathcal{R} > 1$, system (6) has an additional (unique) positive equilibrium, $\mathbf{X}^*$, that is globally asymptotically stable on $\mathbb{R}^4_+ \setminus \{\mathbf{0}\}$.

The positive equilibrium is a regular equilibrium if $F_p < F_p^*$ and it is a virtual equilibrium if $F_p > F_p^*$.

Remark 3.2. *As already highlighted for the non-delayed system, the threshold F_p^* determines the minimum level of control below which the control has essentially no effect on an established pest population for the delayed model.*

3.2. Case with male scarcity: $\gamma M < F + F_p$

In this case, system (3) becomes

$$\frac{dx}{dt} = f_2(x, x_\tau), \tag{10}$$

The right hand side of system (10) is Lipschitz continuous. Thus, according to the standard theory of Delay Differential Equations [9], system (10) admits a unique local solution for each continuous initial condition $\psi \in \mathcal{C}([-\tau_2, 0], \mathbb{R}^2_+)$. In addition, the following domain

$$\begin{aligned}\Omega := \quad \{x \in \mathbb{R}^4_+ : E \leq K,\ F < \frac{r\,\nu_E\, e^{-\tau_2\mu_L}\, e^{-\tau_3\mu_F}\, K}{\mu_F},\ A \leq \frac{(1-r)\,\gamma\,\nu_F\,\nu_E\, e^{-\tau_2\mu_L}\, K}{\mu_A\,\mu_M},\\ M \leq \frac{(1-r)\,\nu_E\, e^{-\tau_2\mu_L}\, K}{\mu_M}\}\end{aligned} \tag{11}$$

is positively invariant for system (10). Global existence on $[0, +\infty)$ of the solution follows by dissipativity of (10). Then, we derive

Proposition 3.1. *There exits a threshold $F_p^{**} > 0$ of F_p such that*

- *If $F_p > F_p^{**}$ the only equilibrium of system (10) on $\mathbb{R}^4_+$ is $\mathbf{0}$.*
- *If $0 < F_p < F_p^{**}$, system (10) has three equilibria on $\mathbb{R}^4_+$, $\mathbf{0}$ and two positive equilibria.*

In addition, $\mathbf{0}$ is an absolutely stable equilibrium.

Proof : The proof follows the proof of Theorem 4 [4], page 446. However, for reader's convenience we provide it in Appendix B, page 18, with additional explanations.

□

Similarly, we show

Theorem 3.3 (Bifurcation Study of F_p^* and F_p^{**}). *Let $F_p > 0$. The following holds for system (2):*

- **0** *is an absolutely stable equilibrium.*
- *If $0 < F_p < F_p^*$, there are two positive equilibria $X^{(1)}$ and X^*, where X^* is asymptotically stable.*
- *If $F_p^* < F_p < F_p^{**}$, there are two positive equilibria $X^{(1)}$ and $X^{(2)}$.*
- *If $F_p > F_p^{**}$, there is no positive equilibrium*

Proof : The proof follows the proof of Theorem 15 [4], page 449. However, for reader's convenience we provide it in Appendix C, page 19.

□

The stability properties of $X^{(1)}$ and $X^{(2)}$ are not easy to obtain theoretically. However, numerical simulations show that $X^{(1)}$ is unstable while $X^{(2)}$ is stable. Also, when $F_p > F_p^{**}$, **0** is Globally Asymptotically Stable. As F_p increases and passes through F_p^* the regular equilibrium X^* collides with the virtual equilibrium $X^{(2)}$, such that X^* becomes virtual and $X^{(2)}$ becomes regular. The bifurcation diagram in Fig. 4, page 8, summarizes the previous properties, where the equilibrium values of $F + A$ are given as function of the bifurcation parameter F_p. The blue (red) solid line represents locally (globally) asymptotically stable equilibria, while the blue dotted line represents unstable equilibria.

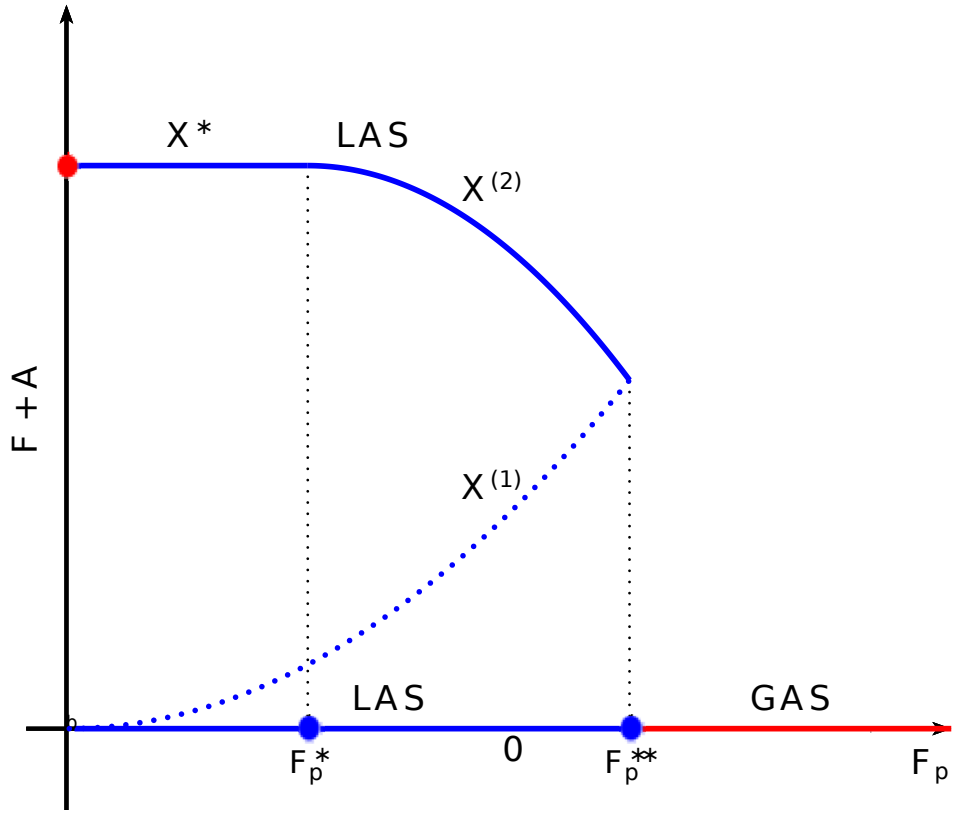

Figure 4: Bifurcation diagram of the values of $F + A$ at equilibrium with respect to the values of F_p for system (2)

About the long term behavior of system (2) when $F_p > 0$

The previous Theorem shows us that the dynamics of the system may vary according to the level of control. In particular, as long as $0 < F_p < F_p^*$, the control has essentially no effect on an established population. Even if $F_p^* < F_p < F_p^{**}$, the effect are negligeable (on an established population). Here, we intend to derive results that may help us to define appropriate control strategies.

Due to the term $-\nu_F \dfrac{\gamma\, M(t)}{F(t)+F_p}\, F(t)$ in (5), the right hand side of (10) is not quasi-monotone. By removing this nonlinear term, we obtain an upper DDE system, that admits a unique positive solution $\overline{x}$ that is an upper solution of system (10). Since $f_2(x,y)$ is nondecreasing in y, according to Theorem 3.6 in [12], page 29, we deduce that $x \leq \bar{x}$.

Thus, following [4], we consider the following upper system, as an auxiliary system of system (10):

$$\frac{dx}{dt} = g_2(x, x_\tau), \tag{12}$$

with $x = (E, F, A, M)^T$ and

$$g_2(x, x_\tau) = \begin{pmatrix} b\, e^{-\tau_3\, \mu_A}\, A(t-\tau_3) \left(1 - \dfrac{E(t)}{K}\right) - (\nu_E + \mu_E)\, E(t) \\ r\, \nu_E\, e^{-\tau_2\, \mu_L}\, E(t-\tau_2) - \mu_F\, F(t) \\ \nu_F\, \dfrac{\gamma\, M(t)}{F(t)+F_p}\, F(t) - \mu_A\, A(t) \\ 1-r)\, \nu_E\, e^{-\tau_2\, \mu_L}\, E(t-\tau_2) - \left(\mu_A + \alpha \dfrac{F_p}{F(t)+F_p}\right) M(t) \end{pmatrix} \tag{13}$$

System (12) is a cooperative time delayed system: the (QM) condition is verified. Hence, the stability of each equilibrium for the non delayed system is preserved for the delayed system. It suffices to study the non delayed system to deduce the long term behavior of the time delayed system:

$$\frac{dx}{dt} = g_2(x, x_0). \tag{14}$$

Let us first set

$$\mathcal{R}_M = \frac{(1-r)\, b\, \nu_E\, \gamma \nu_F\, e^{-\tau_2\, \mu_L}\, e^{-\tau_3\, \mu_A}}{\mu_A\, (\nu_E + \mu_E)\, \mu_M} \tag{15}$$

While $\mathcal{R}$, the basic offspring number, represents the number of offsprings produced by one single female during its mean lifespan, $\mathcal{R}_M$ represents the number of offsprings produced by one male during its mean lifespan.

We show the following

Theorem 3.4. *(1) The non delayed system (14) defines a positive dynamical system on $\mathbb{R}^4_+$.*

(2) There exists a threshold value $\bar{F}_p^{**}$ such that

- *(i) if $F_p > \bar{F}_p^{**}$, $\mathbf{0}$ is GAS on $\mathbb{R}^4_+$.*
- *(ii) if $F_p = \bar{F}_p^{**}$, and $\mathcal{R}_M > 1$, then system (14) has two equilibria: $\mathbf{0}$ and one positive equilibria $\bar{X}_1$. The basin of attraction of trivial equilibrium contains the set $\{x \in \mathbb{R}^4_+ : 0 \leq x < \bar{X}_1\}$. The basin of attraction of $\bar{X}_1$ contains the set $\{x \in \mathbb{R}^4_+ : x \geq \bar{X}_1, E \leq K\}$.*
- *(iii) if $0 < F_p < \bar{F}_p^{**}$, and $\mathcal{R}_M > 1$, then system (14) has three equilibria: $\mathbf{0}$ and two positive equilibria $\bar{X}_1$ and $\bar{X}_2$ such that $\bar{X}_1 < \bar{X}_2$. The basin of attraction of $\mathbf{0}$ contains the set $\{x \in \mathbb{R}^4_+ : 0 \leq x < \bar{X}_1\}$. The basin of attraction of $\bar{X}_2$ contains the set $\{x \in \mathbb{R}^4_+ : x \geq \bar{X}_2, E \leq K\}$.*

Proof : See Appendix D, page 21.

□

Using the previous results, and assuming $\mathcal{R} > 1$ and $\mathcal{R}_M > 1$, we can deduce the following results for the delayed system (12)

Theorem 3.5. *There exists a threshold value* $\overline{F}_p^{**}$ *such that*

(i) if $F_p > \overline{F}_p^{**}$, $\mathbf{0}$ *is the only equilibrium for the system (12)*

(ii) if $0 < F_p < \overline{F}_p^{**}$, $\mathcal{R} > 1$, *and* $\mathcal{R} > \dfrac{\mu_M r}{(1-r)(\nu_F+\mu_F)\gamma}$, *we have* $\bar{E}_1$, $\bar{E}_2 \in [0, K]$.*the system has three equilibria: trivial equilibrium* $\mathbf{0}$ *and two positive equilibria* $\bar{X}_1$ *and* $\bar{X}_2$ *such that* $\bar{X}_1 < \bar{X}_2$.

Since model (12) is a delayed cooperative model, we can deduce from [4] the following result about the stability of equilibria:

Theorem 3.6. *Let* $F_p > 0$. *Then, the following holds for the model (12):*

- *If* $0 < F_p \leq \overline{F}_p^{**}$, *then the basin of attraction of the trivial equilibrium contains* $\{x \in \mathbb{R}_+^4 : x \leq \bar{X}_{1,F_p}\}$.
- *If* $F_p \geq \overline{F}_p^{**}$, *then trivial equilibrium is GAS on* $\mathbb{R}_+^4$.

Finally we can deduce the following GAS result for the PWS-DDE system (3) (or system (2))

Theorem 3.7. *Let* $F_p > 0$ *then the following hold for the model (2):*

- *If* $0 < F_p \leq \overline{F}_p^{**}$, *then the basin of attraction of* $\mathbf{0}$ *contains* $\{x \in \mathbb{R}_+^4 : x \leq \bar{X}_{1,F_p}\}$.
- *If* $F_p \geq \overline{F}_p^{**}$, *then* $\mathbf{0}$ *is GAS on* $\mathbb{R}_+^4$.

In fact, the last theorem is very useful to derive a long term control strategy. Indeed, if the control stops, the system will automatically recover. In the other hand, using only long time massive releases of pheromones is not a sustainable option. However, we know that once the non-massive control starts, i.e. $0 < F_p < \overline{F}_p^{**}$, the system become bistable, such that locally, at least in $\{x \in \mathbb{R}_+^4 : x \leq \bar{X}_{1,F_p}\}$, $\mathbf{0}$ is stable and attractive, for a given (small) amount of pheromones, F_p.

3.3. On an long term control strategy related to the level of infestation of Mirids

The previous theoretical results lead to two strategies for long term control

- When the mirid population is small or at an invading stage (not established in the field, but starting to settle), thanks to the size of the plot, a limited number of traps (releasing a small amount of pheromones) can be sufficient to control it. In other words, knowing the population size, it could be possible to estimate F_p, with $0 < F_p < \overline{F}_p^{**}$, such that the mirid population stays in $[\mathbf{0}, \mathbf{X_{1,F_p}}[$, i.e. inside the basin of attraction of $\mathbf{0}$.
- When the population is large, at equilibrium for instance, then, to reduce sharply the population, we need to increase the number of traps in order to release enough pheromones/Fake females, using the GAS property of $\mathbf{0}$ when $F_p > \overline{F}_p^{**}$. This is what we called the "maximal treatment". Thus, according to the GAS of $\mathbf{0}$, there exists $t^* > 0$, such that for $t > t^*$, the mirid population becomes small enough that a small amount of pheromones is sufficient to maintain the population under a given threshold, here $X^{(1)}$, the lowest equilibrium for a given (small preferably) amount of pheromones $F_p << \overline{F}_p^{**}$. This is what we called the "minimal treatment". Altogether, when the population is large, the best way to control it is to first start the control with the "maximal treatment", followed by the "minimal treatment".

  To summarize the "maximal-minimal treatment" strategy: for a given large amount of pheromones, $F_p > \overline{F}_p^{**}$, it suffices to estimates the time, t^*, necessary to enter $[\mathbf{0}, X^{(1}[$, where $X^{(1}$ is estimated for a given small amount of pheromones, $F_p^{(1)} << \overline{F}_p^{**}$. Since $X^{(1)}$ cannot be estimated analytically, we can only estimate the minimum time, t^*, numerically. This is what is illustrated in the next subsection.

b	r	K	$1/\nu_L$	$1/\nu_F$	μ_L	μ_A	μ_M	μ_F	μ_E
3.28	0.58	5000	25	10	0.01	0.08	0.08	0.08	0.001

α	γ	$1/\nu_E = \tau_1$	τ_2	τ_3
0.1	1	15	25	10

Table 2: Values used for simulations of model (2) with $\mathcal{R} > 1$ [1] and $\mathcal{R}_M > 1$

3.4. Applications - Numerical simulations

In this section, we will prove numerically the theoretical results obtained. The values used for the next simulations are given in Table 2, page 11 (taken from [1]), leading to the case $\mathcal{R} = 4.5547 > 1$ and $\mathcal{R}_M = 7.4211$.

According to the theoretical part and the parameters values, for a maximal control, we need to release more than $\overline{F}_p^{**} \approx 1162$ fake females (per ha), in other words for any value of F_p larger than $\overline{F}_p^{**}$, the system will converge to $\mathbf{0}$ for t sufficiently large. However, as explained above, we are not interested in a permanent maximal treatment, but we only want to reach (rapidly) a level of population where the damages can be acceptable and where the population can be controlled with a small amount of pheromones. That is why we choose $F_p^{(1)}$ to estimate $\mathbf{X^{(1)}}$ and thus target the box $[\mathbf{0}, \mathbf{X^{(1)}} - \epsilon]$, for a given $0 < \epsilon << 1$.

In the sequel, we initiate the simulations at the wild equilibrium. We choose $F_p = 100$ such that we estimate numerically $X^{(1)} = (95.1836, 35.8291, 4.4550, 13.5112)$ (the red dot in Fig. 6, page 12). Hence, in the next simulations, for a given $F_p > \overline{F}_p^{**}$, we estimate the minimum time necessary to enter $[\mathbf{0}, X^{(1)} - \epsilon]$. In Figs. 5 and 6, page 11, we present an example of the control strategy described above:

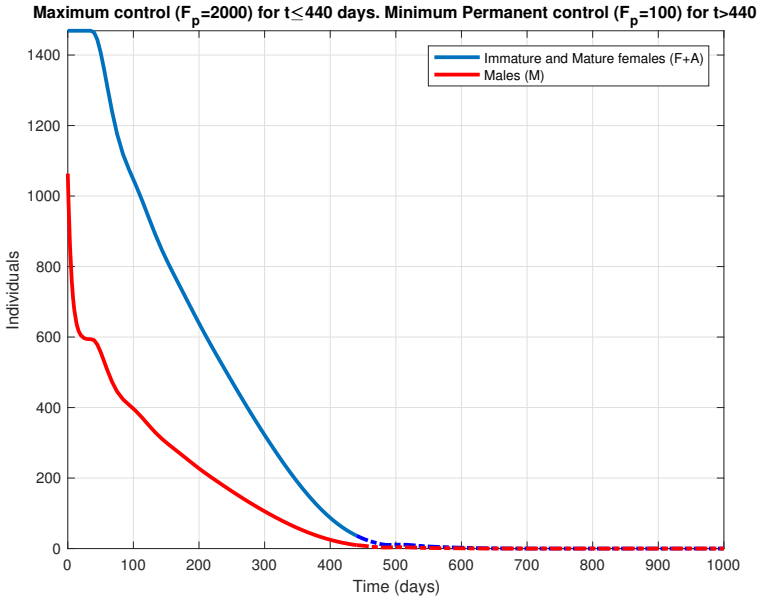

Figure 5: Mating disruption and Trapping Control with, first $F_p = 2000$ (solid lines), then $F_p = 100$ (dotted lines) once the system has reach $[\mathbf{0}, \mathbf{X^{(1)}}[$.

first, we consider a large amount of pheromones traps, such that $F_p = 2000$, to use the GAS property of $\mathbf{0}$, in order to reach the box $[\mathbf{0}, \mathbf{X^{(1)}}[$, where $X^{(1)}$ is estimated based on the targeted level of control, i.e. $F_p^{(1)} = 100$. Numerically, we estimate that 440 days of maximum treatment are necessary to enter the basin $[\mathbf{0}, \mathbf{X^{(1)}}[$. Then, for all $t > 440$ days, we remove some pheromones traps in order to reach the value $F_p^{(1)} = 100$: the system continues to converge to $\mathbf{0}$, thanks to the LAS property of $\mathbf{0}$ in $[\mathbf{0}, \mathbf{X^{(1)}}[$, when $F_p^{(1)} = 100$.

Note, that the previous results correspond to the case when male trapping occurs, $\alpha = 0.1$. If we

assume that there is no trapping, i.e. $\alpha = 0$, then the $M_{T_1} \approx 3576$, and also the minimal time necessary to enter the basin $[\mathbf{0}, X^{(1)}[$ increases to 536 days but we have to use the double amount of pheromones (fake females) $M_T = 4000$. That is why the combination of mating disruption and trapping is of utmost importance, not only to minimize the duration of the treatment but also to minimize the release of pheromones.

Fig. 6(a), page 12, shows different phase of the control: a first phase, where only the male population is reducing, then the eggs population, before the whole system $(E + F + A + M)$ starts to decay. This shows that in constant environmental conditions (constant parameters) the duration of the control is crucial. In Fig. 6(b), page 12, the green box represents the basin $[\mathbf{0}, \mathbf{X^{(1)}}]$: the red trajectory represents the trajectory when the control is defined by $F_p = 100$. Of course, in that case, since $\mathbf{0}$ is LAS in $[\mathbf{0}, \mathbf{X^{(1)}}]$, the system continues to decay (slowly) to $\mathbf{0}$. Of course, the time necessary to enter the basin $[\mathbf{0}, \mathbf{X^{(1)}}]$

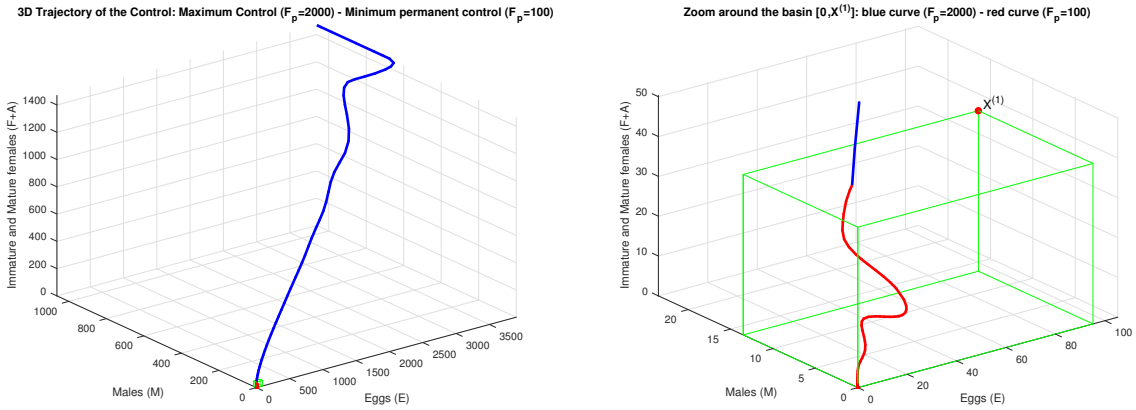

Figure 6: Maximal Control with, first, $F_p = 2000$ (blue solid line), then, once the system has reach $[\mathbf{0}, \mathbf{X^{(1)}}[$, the minimal control starts with $F_p = 100$. The system continues to converge to $\mathbf{0}$ (red solid line), but slowly.

depends on the initial maximum control, the larger, the shorter the time needed. However, as showed in Fig. 7, page 13, it seems that choosing F_p between 2000 and 4000 provides the more interesting results. However, the cost of pheromones need to be taken into account in order to derive the best strategies. The previous strategy is based on two given values for F_p. Other strategies based on the use of several values for F_p could be chosen in order to reduce progressively the amount of pheromones and to use the LAS of $\mathbf{0}$ in the box $[\mathbf{0}, \mathbf{X^{(1)}_{F_p}}]$, for a given F_p. However, from a practical point of view, reducing F_p, while convenient on the paper, seems to be more difficult from a practical point of view.

4. About mating disruption strategy when the pods carrying capacity is periodic

Like in [1], we have to consider that the mirid population dynamics is mainly related to the presence/absence of pods, but not only. Indeed, the cacao production in Cameroon is seasonal, which is not the case, for instance, in Central America. Thus, in Cameroon, the pods carrying capacity, K, is not constant but has to be approximated by a yearly periodic function. Last but not least, we know that, in the absence of pods, mirids can maintain in the area using secondary host plants, like *Cola nitida*, or *Ceiba pentandra* [1]. Thus finally, we consider the following pods carrying capacity $K(t) + C$, where $C > 0$ is a given constant, equal to 100 [1], and $K(t)$ is defined as in [1] (see Table E.3, page 23).

In that case, the control strategy is rather different than in the constant coefficients case. Here, knowing the inter-period (from March to June), when no cocoa pods are available, is rather crucial: it seems obvious to start the control at the beginning of this period , i.e. in March, in order to use the LAS property of model (3), when $K(t) \equiv 0$, to avoid the establishment of the mirid population within the cocoa plantation when $K(t)$ rises again (in July).

We thus consider the following non-autonomous periodic DDE-PWS system

$$\frac{dx}{dt} = f(x, x_\tau, t) := \begin{cases} f_1(x, x_{\tau_2}, x_{\tau_3}, t) & \text{if} \quad F + F_p \leq \gamma\, M \\ f_2(x, x_{\tau_2}, x_{\tau_3}, t) & \text{if} \quad F + F_p \geq \gamma\, M \end{cases} \tag{16}$$

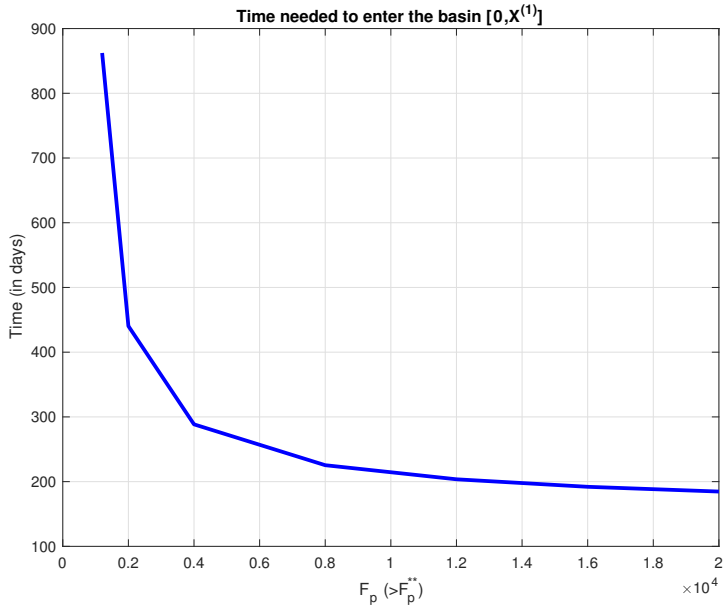

Figure 7: Time needed to enter the basin $[\mathbf{0}, \mathbf{X}^{(\mathbf{1})}_{\mathbf{F_p}}]$ for a given $F_p > F_p^{**}$.

where $x = (E, F, A, M)^t$,

$$f_{1,per}(x, x_\tau, t) = \begin{pmatrix} b\, e^{-\tau_3\, \mu_A}\, A(t-\tau_3) \left(1 - \dfrac{E(t)}{C + K(t)}\right) - (\nu_E + \mu_E)\, E(t) \\ r\, \nu_E\, e^{-\tau_2\, \mu_L}, E(t-\tau_2) - (\nu_F + \mu_F)\, F(t) \\ \nu_F\, F(t) - \mu_A\, A(t) \\ (1-r)\, \nu_E\, e^{-\tau_2\, \mu_L}\, E(t-\tau_2) - \left(\mu_M + \alpha \dfrac{F_p}{F(t) + F_p}\right) M(t) \end{pmatrix} \tag{17}$$

and

$$f_{2,per}(x, x_\tau, t) = \begin{pmatrix} b\, e^{-\tau_3\, \mu_A}\, A(t-\tau_3) \left(1 - \dfrac{E(t)}{C + K(t)}\right) - (\nu_E + \mu_E)\, E(t) \\ r\, \nu_E\, e^{-\tau_2\, \mu_L}\, E(t-\tau_2) - \nu_F \gamma \dfrac{M(t)}{F(t) + F_p}\, F(t) - \mu_F\, F(t) \\ \nu_F\, \gamma \dfrac{F(t)}{F(t) + F_p}\, M(t) - \mu_A\, A(t) \\ 1-r)\, \nu_E\, e^{-\tau_2\, \mu_L}\, E(t-\tau_2) - \left(\mu_M + \alpha \dfrac{F_p}{F(t) + F_p}\right) M(t) \end{pmatrix} \tag{18}$$

The methodology to study the periodic PWS-DDE (16) follows the methodology of the previous sections, thanks to the fact that $0 < C \leq K(t) \leq K_{\max} + C$. Indeed, for $i = 1, 2$, it is straightforward to check that

$$f_{i,C}(x, x_\tau) \leq f_{i,per}(x, x_\tau, t) \leq f_{i,C+K_{\max}}(x, x_\tau), \quad \text{for all } t > 0. \tag{19}$$

1. In the male abundance case, $f_{1,C}$ and $f_{1,C+K_{\max}}$ are delayed system that verify the (QM) condition. Thus, using (19), and applying Theorem 5.1.1 [10], we deduce that

$$x_{1,C}(t) \leq x_{1,per}(t) \leq x_{1,C+K_{\max}}(t), \quad \text{for all } t > 0.$$

where $x_{1,per}$ is the solution of the periodic male abundance equation, $x_{1,C}$ and $x_{1,C+K_{\max}}$ are respectively solutions of the autonomous male abundance system (6), with $K \equiv C$ and $K \equiv C + K_{\max}$ respectively. Thus, using Theorem 3.2, page 7, we can deduce

Theorem 4.1. • *Assume $\mathcal{R}_0 < 1$, then $x_{1,per}$ converges to $\mathbf{0}$.*

- *Assume $\mathcal{R}_0 > 1$, then the male abundance system is permanent, i.e. $x_{1,per} > 0$ for all $t > 0$.*

where $\mathcal{R}_0$ is defined in (8).

Remark 4.1. *Following [1], when $\mathcal{R}_0 > 1$, it is possible to show that the male abundance system converges to a unique periodic solution, $x^*_{per}(t)$, defined as follows:*

$$E^*_{per}(t) = \left(1 - \frac{1}{\mathcal{R}}\right)(C + K(t)), \quad F^*_{per}(t) = \frac{r\,\nu_E\,e^{-\tau_2\,\mu_L}}{\mu_F + \nu_F}\,E^*_{per}(t),$$

$$A^*_{per}(t) = \frac{\nu_F}{\mu_A}\,F^*_{per}(t), \quad M^*_{per}(t) = \frac{(1-r)\,\nu_E\,e^{-\tau_2\,\mu_L}}{\mu_M + \alpha\,\dfrac{F_p}{F^*_{per}(t) + F_p}}\,E^*_{per}(t).$$

2. The male scarcity case is rather more difficult to study. However, we can use the second inequality in (19): $f_{2,per}(t, x, y)$ is nondecreasing in y; thus, according to Theorem 3.6 in [12], page 29, we deduce that $x_{2,per} \leq x_{2,C+K_{\max}}$, such that the methodology developed in section 3.2, page 7, can be applied to the system

$$\frac{dx}{dt} = f_{2,C+K_{\max}}(x, x_\tau).$$

Hence, we deduce that there exists $\overline{F}^{**}_{p,C+K_{\max}} > 0$ such that $\mathbf{0}$ is GAS when $F_p > \overline{F}^{**}_{p,C+K_{\max}} > 0$, i.e. $x_{2,C+K_{\max}}$ converges to $\mathbf{0}$ and so is $x_{2,per}$ as t goes to $+\infty$.
However, for a practical application, this result is not interesting since the amount of pheromones to release can be very large.
Another possibility is to focus on the case where $K \equiv 0$ from March to June, such that we know that periodic system reduces to the autonomous system with carrying capacity C, in other word: $f_{i,per}(x, x_\tau) = f_{i,C}(x, x_\tau)$. In that case, we are able to estimate $\overline{F}^{**}_{p,C}$. When $C = 100$, then $\overline{F}^{**}_{p,C} \approx 23.23$

4.1. Periodic case - Simulations

As explained above we focus on the period from March to June, i.e, we adapt the starting time of our control: either a the end of Period or at the beginning.

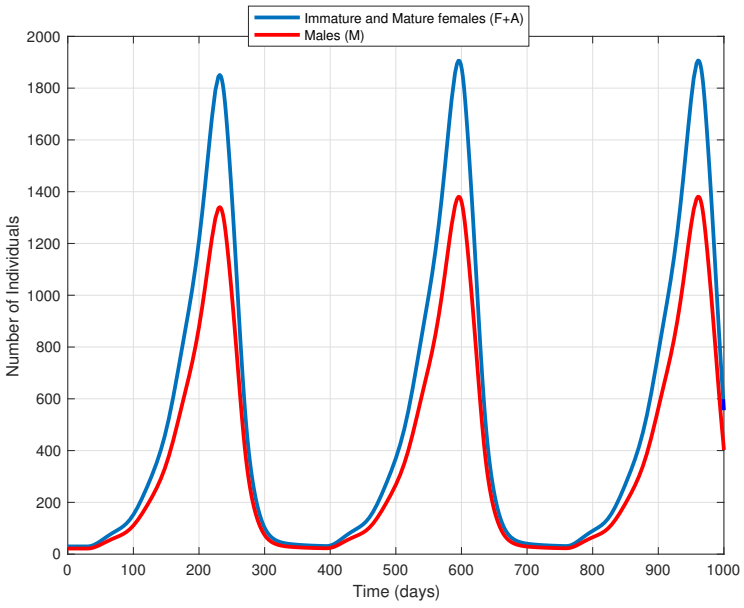

Figure 8: Time evolution of the periodic system, without control

Then, we consider two starting times: $t = 390$ (beginning of July), see Fig. 9, page 15; and $t = 300$ (beginning of March), see Fig. 10, page 15. When choosing $F_p = 20$ as the targeted amount of

pheromones, we are looking at the time t^* necessary to enter and also stay inside $[\mathbf{0}, X^{(1)}[$, with $X^{(1)} = (27.11, 10.20, 1.70, 4.04)$.
As illustrated in Fig. 9, page 15, starting lately within the no-production period, at $t_{start} = 390$, will have an effect during the production period, with a population fourth times less than without control, and it is only after 470 days of $F_p = 100$ treatment that the trajectory enter the box $[\mathbf{0}, X^{(1)}[$ and then continues to decay to zero with $F_p = 20$.
In contrary, starting the treatment early, at $t_{start} = 300$, within the no-production period, the population decreases rapidly, and in 217 days, the trajectory enter the box $[\mathbf{0}, X^{(1)}[$ and then continues to decay to zero with $F_p = 20$. In addition, the population has become so small, that even when the pods are back, the mirid population stay within $[\mathbf{0}, X^{(1)}[$, event with a small amount of pheromones, $F_p = 20$.

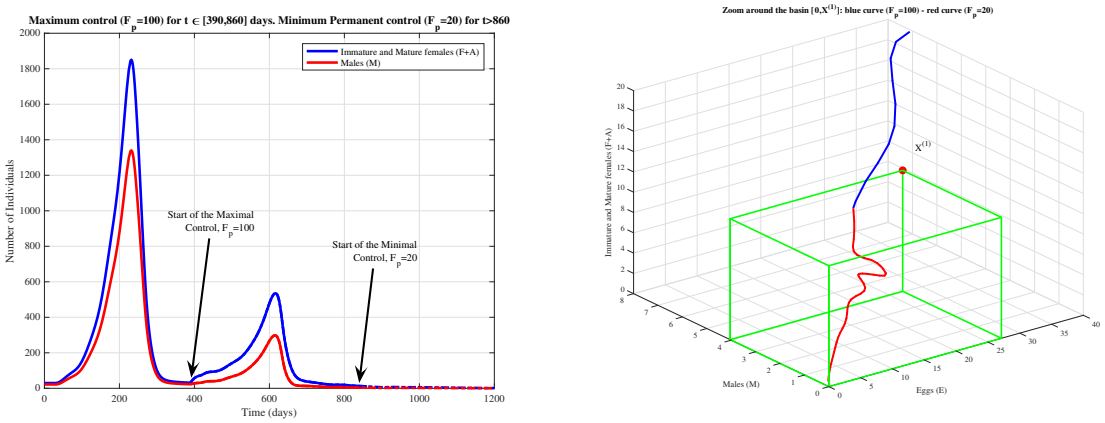

Figure 9: Maximal Control, with $F_p = 100$, then, once the system has reach $[\mathbf{0}, \mathbf{X^{(1)}}[$ at time $t_{max} = 860$, the minimal control starts (dotted lines), with $F_p = 20$: (a) trajectories of the system (b) Zoom of the trajectory near $[\mathbf{0}, X^{(1)}[$ (blue solid line: maximal control; red solid line: minimal control

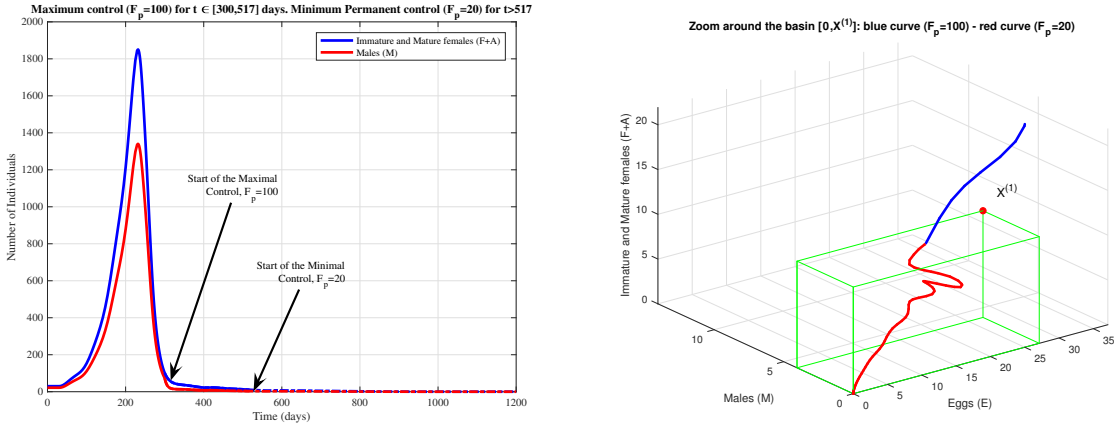

Figure 10: Maximal Control, with $F_p = 100$, then, once the system has reach $[\mathbf{0}, \mathbf{X^{(1)}}[$ at time $t_{max} = 517$, the minimal control starts (dotted lines), with $F_p = 20$, : (a) trajectories of the system (b) Zoom of the trajectory near $[\mathbf{0}, X^{(1)}[$ (blue solid line: maximal control; red solid line: minimal control

In fact, the periodic case, for mating disruption and trapping control, is the most favorable case, as we can use the no-production period, and thus when the mirid population is at its lowest, to be very efficient, especially if the treatment starts early (beginning of March, for instance).

5. Conclusion

We have considered a mating disruption and trapping model to study the opportunity of using sex-pheromones to control a mirid population. We obtain a PWS-DDE model, a kind of model that is not so common in Mathematical Biology. Thanks to the previous works by some of the authors and a suitable use of the Monotone System theory, we were able to provide theoretical results that helped us to provide interesting strategies that could be used in the field for long term control.

Of course, this work provides only partial insight of this complex system. Using a temporal approach, we implicitely assume that mirids and pheromones are homogeneously distributed, which is not the case in the field. A next step would be to take into account the spatial component, like in [13]. Last, but not least, it is well known that mirids aggregate on some particular trees, such that aggregation and dispersion processes should be taken into account, and also the impact of these behaviors in terms of the distribution and the density of the pheromone traps. This may require another modeling approach, thanks to the fact that very few knowledge are available about pheromone spreading, mirid's sensitivity to pheromone, etc.

Acknowledgments

YD acknowledges the (partial) support of the DST/NRF SARChI Chair in Mathematical Models and Methods in Biosciences and Bioengineering at the University of Pretoria (grant 82770).

The authors thank the anonymous reviewers for their fruitful comments that greatly improve the initial manuscript.

Bibliography

[1] M. Djoukwe Tapi, L. Bagny Beilhe, S. Bowong, Y. Dumont, Models for miridae, a cocoa insect pest. application in control strategies, Mathematical Methods in the Applied Sciences 41 (2018) 8673–8696.

[2] R. Mahob, R. Babin, G. ten Hoopen, L. Dibog, D. Hall, C. Bilong Bilong, Field evaluation of synthetic sex pheromone traps for the cocoa mirid sahlbergella singularis (hemiptera: Miridae), Pest management science 67 (6) (2011) 672–676.

[3] J. Sarfo, C. Campbell, D. Hall, Optimal pheromone trap density for mass trapping cacao mirids, Entomologia Experimentalis et Applicata 166 (7) (2018) 565–573. doi:10.1111/eea.12699.

[4] R. Anguelov, C. Dufourd, Y. Dumont, Mathematical model for pest–insect control using mating disruption and trapping, Applied Mathematical Modelling 52 (2017) 437–457.

[5] E. Joseph, Behavioural responses of cocoa mirids, sahlbergella singularis hagl. and distantiella theobroma dist. (heteroptera: Miridae), to sex pheromones, Ph.D. thesis, University of Greenwich (july 2013).

[6] Y. Dumont, J.-M. Tchuenche, Mathematical studies on the sterile insect technique for the Chikungunya disease and *Aedes albopictus*, Journal of Mathematical Biology 65 (5) (2012) 809–855.

[7] M. Strugarek, H. Bossin, Y. Dumont, On the use of the sterile insect release technique to reduce or eliminate mosquito populations, Applied Mathematical Modelling 68 (2019) 443 – 470. doi:https://doi.org/10.1016/j.apm.2018.11.026.

[8] P. Bliman, D. Cardona-Salgado, Y. Dumont, O. Vasilieva, Implementation of control strategies for sterile insect techniques, Mathematical Biosciences 314 (2019) 43 – 60. doi:https://doi.org/10.1016/j.mbs.2019.06.002.

[9] J. Hale, Theory of Functional differential equations, Vol. 3 of Applied Mathematical Sciences, Springer, New York, 1977.

[10] H. Smith, Monotone dynamical systems: An introduction to the theory of competitive and cooperative systems, American Mathematical Society 41.

[11] R. Anguelov, Y. Dumont, J.-S. Lubuma, Mathematical modeling of sterile insect technology for control of anopheles mosquito, Computers and Mathematics with Applications 64 (3) (2012) 374–389.

[12] H. Smith, An Introduction to Delay Differential Equations with Applications to the Life Sciences, Vol. 57 of Texts in Applied Mathematics, Springer, New York Dordrecht Heidelberg London, 2011.

[13] R. Anguelov, C. Dufourd, Y. Dumont, Simulations and parameter estimation of a trap-insect model using a finite element approach, Mathematics and Computers in Simulation 133 (2017) 47–75. doi:https://doi.org/10.1016/j.matcom.2015.06.014.

[14] D. Barton, Stability calculations for piecewise-smooth delay equations., I. J. Bifurcation and Chaos 19 (2009) 639–650. doi:10.1142/S0218127409023263.

[15] M. Bernardo, C. Budd, A. Champneys, P. Kowalczyk, Piecewise-smooth dynamical systems: theory and applications, Vol. 163, Springer Science & Business Media, 2008.

[16] D. Bisselua, Yede, S. Vidal, Dispersion models and sampling of cacao mirid bug Sahlbergella singularis (hemiptera: Miridae) on theobroma cacao in southern cameroon, Environmental Entomology 40(1) (2011) 111–119.

Appendix A. Appendix A: Piecewise smooth (PWS) dynamical systems

We just provides some definitions related to PWS dynamical systems, given in [14]. For a general presentation, the interested readers are referred to [15] or [4].

Definition Appendix A.1. *A piecewise-smooth flow is given by a finite set od ODEs* $\dot{x}_i(t) = F_i(x, \mu)$, $x \in S_i$; *where* $\cup_i S_i = \mathcal{D}$ *is a domain, each* S_i *has a non-empty interior.*

The intersection $\sum_{ij} := S_i \cap S_j$ is either an $\mathbb{R}^{n-1}$-dimensional manifold included in the boundaries ∂S_j and ∂S_i, or is the empty set. Each vector field F_i is smooth in both state x and parameter μ, and defines a smooth flow $\phi_i(x, t)$ within any open set $U \supseteq S_i$.

A non-empty border between two regions $\sum_{ij}$ will be called a discontinuity set, discontinuity boundary, or a switching manifold.

Definition Appendix A.2. *[14] Let* $\dot{x}(t) = f(x(t), x(t-\tau))$ *be a delay dynamical system. A simple example of a PWS-DDE composed of two smooth vector fields is*

$$\dot{x}(t) = \begin{cases} f_1(x(t), x(t-\tau)) & if \quad f(x(t), x(t-\tau)) \leq 0 \\ f_2(x(t), x(t-\tau)) & if \quad f(x(t), x(t-\tau)) \geq 0. \end{cases} \tag{A.1}$$

where $x(t) \in \mathbb{R}^n$, *and* f_1, f_2, f *are sufficiently smooth functions. Transitions between the different vector fields occur on the switching surface defined by* $f = 0$.

Definition Appendix A.3. *[14] We define a PWS-DDE to be a collection of smooth vector fields*

$$\dot{x}(t) = f_m(x^t) \tag{A.2}$$

indexed by a mode variable $m \in \mathcal{M}$ *where* $x^t \in \mathcal{C}([-\tau, 0], \mathbb{R}^n)$ *is the solution segment* $x(t+s)$ *for* $-\tau \leq s \leq 0$ *and* $\mathcal{M}$ *is a finite set. (Equation A.2 encompasses distributed delays as well as discrete delays; however, we deal here with discrete delays only.) Associated with this is a collection of events* $e \in \mathcal{E}$ *where* $\mathcal{E}$ *is a finite set and* e *consists of a pair* $\pi_e = (m_{in}, m_{out})$, *a smooth event function* $h_e(x^t) : \mathcal{C}([-\tau, 0], \mathbb{R}^n) \longleftrightarrow \mathbb{R}$ *and a smooth jump function* $g_e(x^t) : \mathcal{C}([-\tau, 0], \mathbb{R}^n) \longleftrightarrow \mathcal{C}([-\tau, 0], \mathbb{R}^n)$.

The event function $h_e = 0$ implicitly defines a switching manifold marking the transition point between the (potentially) different vector fields $(f_{m_{in}}, f_{m_{out}})$ and the jump function g_e determines the instantaneous change of state that occurs upon impact with the switching manifold. The minimal state needed to uniquely identify a particular trajectory of the system starting at time t_0 is thus x^{t^0} along with the mode m at time t_0.

Definition Appendix A.4. *Following [15], the degree of smoothness at a point* x_0 *in a switching set* $\sum_{ij}$ *of a piecewise-smooth ODE is the highest order* r *such the Taylor series expansions of* $\phi_i(x_0, t)$ *and* $\phi_j(x_0, t)$ *with respect to* t, *evaluated at* $t = 0$,*agree up to terms of* $\mathcal{O}(t^{r-1})$. *That is, the first non-zero partial derivative with respect to* t *of the difference* $[\phi_i(x_0, t) - \phi_j(x_0, t)]|_{t=0}$ *is of order* r.

Appendix B. Appendix: Proof of Proposition 3.1

Setting the left-hand side of system (10) to zero, and after some straightforward calculations, we get the following equation in E to solve:

$$\psi(E) := E\,\xi(E)\,\phi(E) = \eta(F_p, E). \tag{B.1}$$

where

$$\xi(E) = \gamma\,(1-r)\,e^{-\tau_2\,\mu_L}\,\nu_E\,\nu_F\,e^{-\tau_3\,\mu_A}\,b\,\left(1 - \frac{E}{K}\right) - \mu_A\,(\alpha + \mu_M)\,(\nu_E + \mu_E), \tag{B.2}$$

$$\eta(F_p, E) = \mu_A\,\mu_F\,\mu_M\,(\nu_E + \mu_E)\,be^{-\tau_3\,\mu_A}\,\left(1 - \frac{E}{K}\right)\,F_p. \tag{B.3}$$

and

$$\phi(E) = b\,e^{-\tau_3\,\mu_A}\,r\,\nu_E\,e^{-\tau_2\,\mu_L}\,\left(1 - \frac{E}{K}\right) - \mu_A\,(\nu_E + \mu_E).$$

Therefore, assuming that E_{eq} is a positive root of (B.1), the other components of the non trivial equilibria of (10) are:

$$F_{eq} = \frac{\phi(E_{eq})}{\mu_F b e^{-\mu_A \tau_3}\left(1-\dfrac{E_{eq}}{K}\right)} E_{eq}, \tag{B.4}$$

$$A_{eq} = \frac{(\nu_E+\mu_E)}{e^{-\tau_3\,\mu_A} b\,\left(1-\dfrac{E_{eq}}{K}\right)}\,E_{eq}, \tag{B.5}$$

$$M_{eq} = \frac{(1-r)\,\nu_E\,e^{-\tau_2\,\mu_L}}{\mu_M+\alpha\,\dfrac{F_p}{F_{eq}+F_p}}\,E_{eq}. \tag{B.6}$$

Further, to ensure $F_{eq} > 0$, we need to have $\phi(E_{eq}) > 0$, that is E_{eq} must satisfy the condition:

$$E_{eq} < K\,\left(1-\frac{\mu_A\,(\nu_E+\mu_E)}{r\,b\,\nu_E\,e^{-\tau_2\,\mu_L}\,e^{-\tau_3\,\mu_F}}\right) \tag{B.7}$$

In fact, according to the definition of $\psi(E)$, it is straightforward to check that ψ admits two real positive roots in $[0, K]$,

$$E_1 = \left(1-\frac{\mu_A\,(\nu_E+\mu_E)}{b\,e^{-\tau_3\,\mu_A}\,r\,\nu_E\,e^{-\tau_2\,\mu_L}}\right)K, \quad \text{and } E_2 = \left(1-\frac{\mu_A\,(\alpha+\mu_M)\,(\nu_E+\mu_E)}{\gamma\,(1-r)\,e^{-\tau_2\,\mu_L}\nu_E\,\nu_F\,e^{-\tau_3\,\mu_A}b}\right)K,$$

provided that $\dfrac{\mu_A\,(\nu_E+\mu_E)}{b\,e^{-\tau_3\,\mu_A}\,r\,\nu_E\,e^{-\tau_2\,\mu_L}} < 1$ and $\dfrac{\mu_A\,(\alpha+\mu_M)\,(\nu_E+\mu_E)}{\gamma\,(1-r)\,e^{-\tau_2\,\mu_L}\nu_E\,\nu_F\,e^{-\tau_3\,\mu_A}b} < 1$.

Thus, only the points of intersection between the straight line $\eta(F_p, E)$ and the cubic $\psi(E)$ that belong to $[0, \min\{E_1, E_2\}]$ are of interest for us: see Fig. B.11, page 20. We denote by F_p^{**} the value of F_p such that the straight line $\eta(F_p, E)$ is tangent to the indicated section of the graph $\psi(E)$. Then, it is clear that for $F_p > F_p^{**}$ there is no intersection between $\eta(F_p, E)$ and Ψ (no positive equilibrium) while for $0 < F_p < F_p^{**}$, there are two points of intersection (2 positive equilibria).

Finally, straightforward computations show that $\mathbf{0}$ is an absolutely stable equilibrium of system (10).

Appendix C. Appendix: Proof of Theorem 3.3

Assume $0 < F_p < F_p^{**}$. Then, let $E_{eq}^{(1)}$ and $E_{eq}^{(2)}$, $E_{eq}^{(1)} < E_{eq}^{(2)}$ be the roots of (B.1). We denote the respective equilibria by $X^{(1)}$ and $X^{(2)}$. To show that any equilibrium of (10) is a regular equilibrium of (2), we need to show that it belongs to the male scarcity region. Using the previous relationships, it suffices to study the sign of $F_{eq} + F_p - \gamma M_{eq}$. In fact, we can show that

$$F_{eq}+F_p-\gamma M_{eq} = \frac{1}{\mu_M+\alpha\dfrac{F_p}{F_{eq}+F_p}}\left(\mu_M\,(F_{eq}+F_p)+\alpha F_p-\gamma(1-r)\nu_E e^{-\tau_2\mu_L}E_q\right)$$

Thus, studying the sign of $F_{eq} + F_p - \gamma M_{eq}$ is equivalent to study the sign of

$$\left(\mu_M F_{eq}-\gamma(1-r)\nu_E e^{-\tau_2\mu_L}E_q\right)+(\alpha+\mu_M)\,F_p.$$

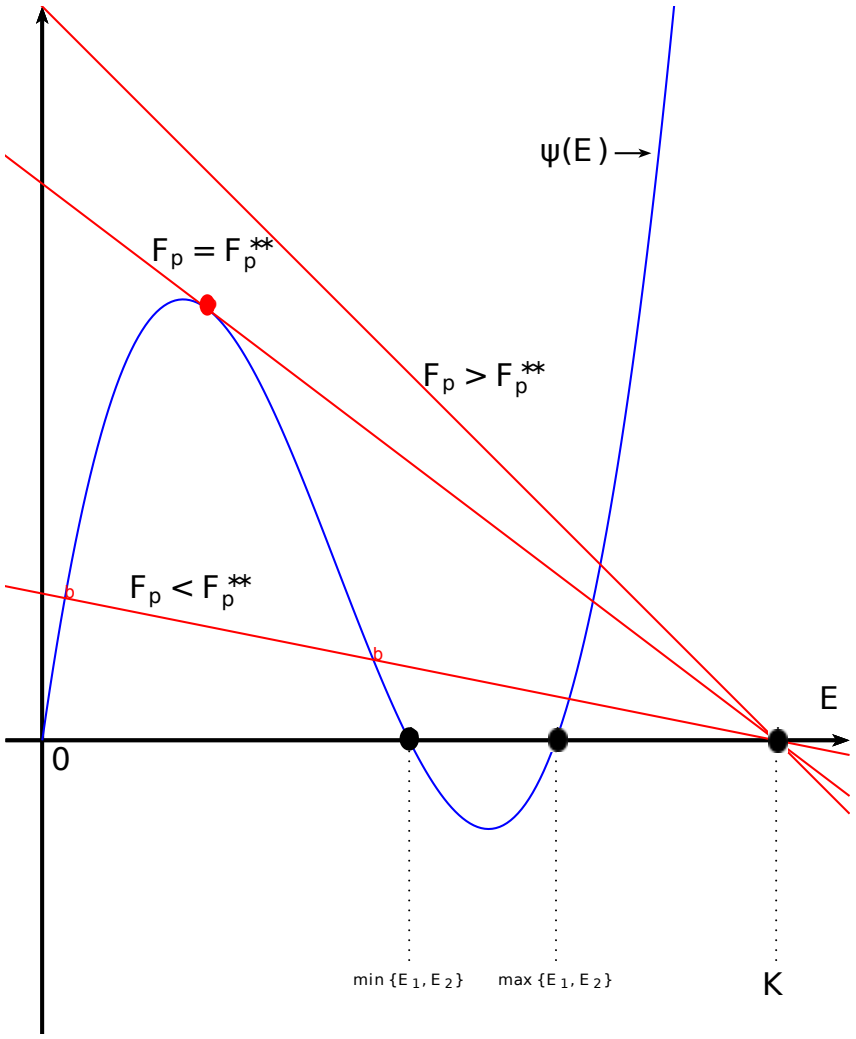

Figure B.11: Intersection between $\psi(E)$ (in blue) and $\eta(F_p, E)$ (in red) for three values of F_p.

In fact we have

$$\left(\mu_M F_{eq} - \gamma(1-r)\nu_E e^{-\tau_2 \mu_L} E_q\right) + (\alpha + \mu_M) F_p = \tag{C.1}$$

$$= \left(\mu_M \frac{\phi(E_{eq})}{\mu_F b e^{-\mu_A \tau_3} \left(1 - \frac{E_{eq}}{K}\right)} - \gamma(1-r)\nu_E e^{-\tau_2 \mu_L} \right) E_q + (\alpha + \mu_M) F_p \tag{C.2}$$

$$= r\,\nu_E\, e^{-\tau_2\,\mu_L} \left(\frac{r\mu_M}{\mu_F} - \frac{\mu_M \mu_A\,(\nu_E + \mu_E)}{\mu_F b e^{-\mu_A \tau_3} \left(1 - \frac{E_{eq}}{K}\right)} - \gamma(1-r) \right) E_q + (\alpha + \mu_M) F_p \tag{C.3}$$

using the inequality $E_{eq}^{(1)} < E_{eq}^{(2)} < E^*$, we have:

$$\geq r\,\nu_E\, e^{-\tau_2\,\mu_L} \left(\frac{r\mu_M}{\mu_F} - \frac{\mu_M \mu_A\,(\nu_E + \mu_E)}{\mu_F b e^{-\mu_A \tau_3} \left(1 - \frac{E^*}{K}\right)} - \gamma(1-r) \right) E_q + (\alpha + \mu_M) F_p$$

$$= r\,\nu_E\,e^{-\tau_2\,\mu_L}\left(\frac{r\mu_M}{\mu_F}-\frac{\mu_M\mu_A\,(\nu_E+\mu_E)\mathcal{R}}{\mu_F b e^{-\mu_A\tau_3}}-\gamma(1-r)\right)E_q+(\alpha+\mu_M)\,F_p$$

and after some simplifications

$$= r\,\nu_E\,e^{-\tau_2\,\mu_L}\left(\frac{r\mu_M}{\mu_F+\nu_F}-\gamma(1-r)\right)E_q+(\alpha+\mu_M)\,F_p.$$

Using (9), page 7, we deduce

$$\left(\mu_M F_{eq}-\gamma(1-r)\nu_E e^{-\tau_2\mu_L}E_q\right)+(\alpha+\mu_M)\,F_p=\frac{(\alpha+\mu_M)}{E^*}\left(F_pE^*-E_qF_p^*\right).$$

Since $E_{eq}^{(1)}<E_{eq}^{(2)}<E^*$, then $F_pE^*-E_qF_p^*>\left(F_p-F_p^*\right)E_q$. Using the fact that $F_p^*<F_p$, then $F_pE^*-E_qF_p^*>0$, such that $F_{eq}+F_p-\gamma M_{eq}>0$. Therefore, in this case, $X^{(1)}$ and $X^{(2)}$ are both in the male scarcity region. Hence, they are also equilibria of (2).
If $F_p<F_p^*$ and $E_{eq}>E^*$, considering the fact that for $0<F_p<F_p^*$, we have $E_{eq}^{(1)}<E^*<E_{eq}^{(2)}$ and using the same method as previously, we obtain $F_p+F_{eq}^{(2)}-\gamma\,M_{eq}^{(2)}<0$.
Therefore, $X^{(2)}$ is not in the male scarcity region. Hence, it is not an equilibrium of (2). Taking into consideration the previous results regarding $X^{(1)}$ and $X^{(2)}$, the theorem is proved.

Appendix D. Appendix: Proof of Theorem 3.4

The first assertion is obvious. Setting the first, second, and fourth terms in (13) equal to zero, we derive

$$\bar{F}=\frac{r\,\nu_E\,e^{-\tau_2\mu_L}}{\mu_F}\bar{E},\quad \bar{A}=\frac{(\nu_E+\mu_E)}{b\,e^{-\tau_3\,\mu_A}\left(1-\dfrac{\bar{E}}{K}\right)}\bar{E},\quad \bar{M}=\frac{\left((1-r)\,\nu_E\,e^{-\tau_2\,\mu_L}\right)\left(\bar{F}+F_p\right)}{\mu_M\,\bar{F}+(\mu_M+\alpha)\,F_p}\bar{E}$$

Solving the third equation equal to zero and substituting the expressions for $\bar{F}$, $\bar{A}$ and $\bar{M}$ above, we obtain an equation for $\bar{E}$ in the form

$$E\phi(E)=\eta(F_p,E),\tag{D.1}$$

with

$$\begin{aligned}\eta(F_p,E)&=\mu_M r\nu_E e^{-\tau_2\mu_L}E+\mu_F\,(\alpha+\mu_M)\,F_P\\ \phi(E)&=(\mu_F+\nu_F)(1-r)\nu_E e^{-\tau_2\mu_L}\gamma\mathcal{R}\left(1-\frac{E}{K}\right)\end{aligned}\tag{D.2}$$

In other words, if (D.1) admits roots, they are intersection between a parabola and a straight line: see Fig. D.12, page 22. In fact, solving (D.1) is equivalent to solve the following quadratic equation

$$\begin{aligned}\frac{\mathcal{R}(1-r)\nu_E e^{-\tau_2\mu_L}\,(\nu_F+\mu_F)\,\gamma}{K}E^2+\nu_E e^{-\tau_2\mu_L}\,(\mu_M r-\mathcal{R}(1-r)\,(\nu_F+\mu_F)\,\gamma)\,E+\\ +\mu_F\,(\alpha+\mu_M)\,F_p=0.\end{aligned}$$

Then, we estimate the discriminant

$$\Delta=\left(\nu_E e^{-\tau_2\mu_L}\,(\mu_M r-\mathcal{R}(1-r)\,(\nu_F+\mu_F)\,\gamma)\right)^2-4\frac{\mathcal{R}(1-r)\nu_E e^{-\tau_2\mu_L}\,(\nu_F+\mu_F)\,\gamma}{K}\mu_F\,(\alpha+\mu_M)\,F_p$$

or equivalently

$$\Delta=\left(\nu_E e^{-\tau_2\mu_L}\mu_M r\,(1-\mathcal{R}_M)\right)^2-4\frac{\mathcal{R}(1-r)\nu_E e^{-\tau_2\mu_L}\,(\nu_F+\mu_F)\,\gamma}{K}\mu_F\,(\alpha+\mu_M)\,F_p$$

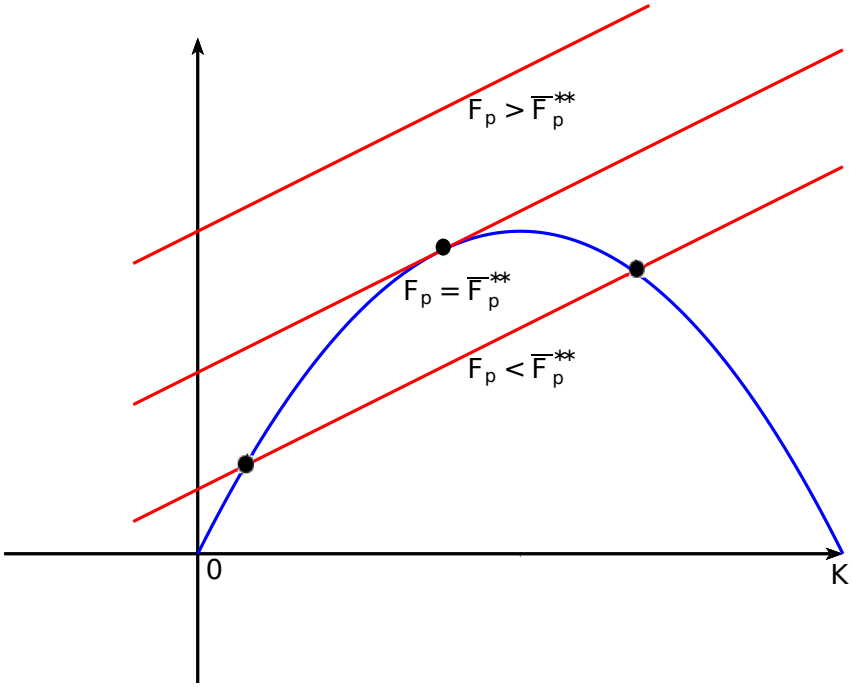

Figure D.12: Intersections between the graphs of $E\phi(E)$ (in blue) and $\eta(F_p, E)$ (in red) for different values of F_p. The black dots represent the intersection points on the interval $[0, K]$.

Clearly, if $F_p > \overline{F}_p^{**}$, with

$$\overline{F}_p^{**} = \frac{\left(\nu_E e^{-\tau_2 \mu_L} \mu_M r \left(1 - \mathcal{R}_M\right)\right)^2}{4\mathcal{R}(1-r)\left(\nu_F + \mu_F\right)\gamma\mu_F\left(\alpha + \mu_M\right)} K,$$

then $\Delta < 0$, and no positive real roots exist. Otherwise, when $F < \overline{F}_p^{**}$, two real roots exist. If in addition, we assume that

$$\mathcal{R}_M > 1,$$

then, we obtain the following positive real roots $\bar{E}_1 < \bar{E}_2$:

$$\bar{E}_1 = \frac{1}{2}\left(\frac{\nu_E e^{-\tau_2\mu_L}\mathcal{R}(1-r)\left(\nu_F + \mu_F\right)\gamma - \mu_M r - \sqrt{\Delta}}{\mathcal{R}(1-r)\nu_E e^{-\tau_2\mu_L}\left(\nu_F + \mu_F\right)\gamma}\right) K$$

$$\bar{E}_2 = \frac{1}{2}\left(\frac{\nu_E e^{-\tau_2\mu_L}\mathcal{R}(1-r)\left(\nu_F + \mu_F\right)\gamma - \mu_M r + \sqrt{\Delta}}{\mathcal{R}(1-r)\nu_E e^{-\tau_2\mu_L}\left(\nu_F + \mu_F\right)\gamma}\right) K.$$

Using (D.1) and (D.2), it is straightforward to show that $\bar{E}_1 < \bar{E}_2 < K$. Assume $F_p > \overline{F}_p^{**}$, then setting

$$\bar{y}_q = \begin{pmatrix} K \\ \dfrac{r\,\nu_E\, e^{-\tau_2\mu_L}}{\mu_F} q \\ \dfrac{\gamma\nu_F(1-r)\,\nu_E\, e^{-\tau_2\,\mu_L}}{\mu_M} \\ \dfrac{(1-r)\,\nu_E\, e^{-\tau_2\,\mu_L}}{\mu_M} \end{pmatrix},$$

where q is any real number, such that $q \geq K$. We check that $g_2(\bar{y}_q, \bar{y}_q) \leq 0$. Thus, by Theorem 7 [4], $\mathbf{0}$ is GAS on $\Omega_K = \bigcup_{q \geq K}[\mathbf{0}, \bar{y}_q]$, which implies that $\mathbf{0}$ is GAS on $\mathbb{R}^4_+$ since Ω_K is an absorbing set.

Appendix E. Biological Data

Following [1], we consider the data issued from [16] for the time evolution of the pods carrying capacity along the year:

Months	Jun	Jul	Aug	Sept	Oct	Nov	Dec	Jan	Feb	Mar	Apr	May	Jun
$K_C(t)$	0	$\frac{32000}{31}$	$\frac{160000}{31}$	$\frac{416000}{30}$	$\frac{544000}{31}$	$\frac{304000}{31}$	$\frac{416000}{31}$	$\frac{120000}{31}$	$\frac{8000}{28}$	0	0	0	0

Table E.3: Daily mean number of cocoa pods